IV International Conference on Particle-based Methods – Fundamentals and Applications
PARTICLES 2015
E. Oñate, M. Bischoff, D.R.J. Owen, P. Wriggers & T. Zohdi (Eds)

A GENERAL METHOD FOR MODELLING DEFORMABLE STRUCTURES IN DEM

A. EFFEINDZOUROU[1], K. THOENI[1], B. CHAREYRE[2] AND A. GIACOMINI[1]

[1]Centre for Geotechnical and Materials Modelling
The University of Newcastle Callaghan, NSW 2308, Australia
http://www.newcastle.edu.au

[2]Laboratoire 3SR
Domaine Universitaire BP53, 38041 Grenoble Cedex 9, France
http://www.3sr-grenoble.fr

Key words: DEM, Cylinder, Grid, Membrane, Arbitrary shape, Minkowsky sum

Abstract. The discrete element method was originally designed to handle rigid spherical particles. In this work, the method is extended to model arbitrary deformable structures, such as membrane and container structures. The paper focuses on the implementation of a deformable discrete element called PFacet (particle facet) in the open-source framework YADE. A PFacet element is geometrically constructed by the Minkowsky sum of a triangular facet and a sphere. Contact detection is based on the three primitives: sphere, cylinder and facet. It allows the representation of arbitrary deformable structures by using the standard contact models for spheres. Finally, the model is validated and an example is presented illustrating the capabilities of the model to simulate arbitrary deformable structures.

1 INTRODUCTION

The discrete element method (DEM) is broadly used to simulate granular materials. The method originally considers the interaction between rigid spheres. The modelling of rounded non-spherical particles allows to take into account the shape of the particles. Indeed, grains in nature and many important phenomena cannot be reproduced just using spherical particles. The simplest method for modelling non-spherical particles is to either bond or clump spheres together [1]. In the first case spheres belonging to the same aggregate interact via a bond where attractive forces are allowed and bonds can brake. In the case of a clump, the aggregate is rigid and the forces on all the spheres making up the clump are added together to obtain the total force. Another way of modelling rounded non-spherical particles is by superquadratic ellipsoids [2] or rounded polyhedra

and spheropolytopes [3]. The latter are discussed more in detail in the following section since a similar concept will be used in the present work. Spheropolytopes are generated from the Minkowski addition of a polytope by a sphere, which is nothing more than the object resulting from sweeping a sphere around a polytope.The idea appeared in [4] for flexible objects and in [5] for convex non-spherical particles. In the latest, a linear triangulation-based contact detection method based on a weighted Delaunay triangulation was used in order to improve the performance. Numerical experiments indicated that the overall complexity of the contact detection is proportional to the number of particles. An extension of the method was published in [6] for simulating non-convex non-spherical particles in 2D. The particle shape was represented by the classical concept of a Minkowski sum, which permits the representation of complex shapes without defining the object as a sum of spherical or convex particles. A well-defined conservative and frictional interaction between these bodies was derived. The method was then extended to 3D by [3].

Starting from the modelling of deformable chained cylinders in 3D [7], this paper presents a general method for modelling deformable non-convex structures with the DEM as published in [8] and implemented into the open-source framework YADE [9]. Firstly, the three primitives used in the model and their implementation are discussed. Then the model is validated and some examples are presented.

2 GENERAL FORMULATION

The contact model of two interacting spheres is presented herein since all possible interactions considered in this work are based on it. The constitutive model used for the sphere–sphere interaction links the relative displacement and relative rotation to the contact force $\vec{F}$ and contact moment $\vec{M}$ acting at the contact between two interacting bodies.

The normal contact force $\vec{F}_n$ and the incremental shear force $\mathrm{d}\vec{F}_s$ are calculated as:

$$\vec{F}_n = \quad k_n \vec{u}_n \tag{1}$$

$$\mathrm{d}\vec{F}_s = \quad k_s \dot{\vec{u}}_s \, \mathrm{d}t \tag{2}$$

where k_n and k_s are the contact stiffnesses associated to the normal and shear force, $\vec{u}_n$ is the normal distance (or overlap) between the two spheres, $\dot{\vec{u}}_s$ is the relative shear velocity, and $\mathrm{d}t$ is the time step.

Considering two spheres S_1 and S_2, the normal and tangential stiffness of the sphere–sphere contact are defined as follows:

$$k_n = \frac{2E_1R_1E_2R_2}{E_1R_1 + E_2R_2} \tag{3}$$

$$k_s = \frac{2E_1R_1\nu_1E_2R_2\nu_2}{E_1R_1\nu_1 + E_2R_2\nu_2} \tag{4}$$

where E_i is the Young's modulus, R_i the radius and ν_i the Poisson's ratio associated to sphere i with $i \in \{1, 2\}$.

The relative rotation of the spheres is used to define the twisting moment $\vec{M}_t$ and the bending moment $\vec{M}_b$. By adopting a vector representation $\vec{\Omega}_{12}$ of the relative rotation, the moments can be calculated as:

$$\vec{M}_t = k_t \vec{\Omega}_{12}^t \tag{5}$$

$$\vec{M}_b = k_b \vec{\Omega}_{12}^b \tag{6}$$

where k_t and k_b are the contact stiffness associated to the twisting and bending moment respectively, and $\vec{\Omega}_{12}^t$ and $\vec{\Omega}_{12}^b$ are the twisting and bending components of the relative rotation associated to the two spheres.

Plastic deformation is taken into account via the following elastic limits:

$$\begin{aligned} \|\vec{F}_n\| &\leq \sigma_n^l A \\ \|\vec{F}_s\| &\leq F_n \tan\varphi + \sigma_s^l A \\ M_t &\leq \frac{\sigma_n^l I_b}{R} \\ M_b &\leq \frac{\sigma_s^l I_t}{R} \end{aligned} \tag{7}$$

where σ_n^l and σ_s^l are the tensile and shear strengths, $\varphi = \min(\varphi_1, \varphi_2)$ is the friction angle, $A = \pi R^2$ is the reference surface area, $I_t = \pi R^4/4$ and $I_b = \pi R^4/8$ are the reference polar and bending moments of inertia respectively, and $R = \min(R_1, R_2)$ is the reference radius of the contact.

3 CYLINDER ELEMENTS

The cylinder element was introduced in [7]. It is the basic entity for the deformable element described in this paper and, hence, it is summarised in this section.

A cylinder is composed of two nodes and a tube. Geometrically it corresponds to the Minkowski sum of a sphere and a polyline. The deformation of a cylinder is characterised by the positions and orientations of its two nodes. The mass of the cylinder element is lumped into its two nodes.

Three types of interactions are considered: sphere–sphere, sphere–cylinder and cylinder–cylinder. The sphere–sphere contact model is used to calculate the sphere–cylinder and cylinder–cylinder interactions. In order to compute the sphere–cylinder interaction, a virtual sphere is introduced. The virtual sphere is centred at the position of the projection of the contact point between the sphere and the cylinder on the segment connecting its nodes. The cylinder and virtual sphere have the same radius. The displacements at the surface of the cylinder are assumed to vary linearly between its nodes. The translational and rotational velocities of the virtual sphere are linearly interpolated between the cylinder's nodes. Then, the forces and moments are distributed on the two nodes.

In [7] chained cylinders (or interconnected cylinders) were used. This allows the modelling of elastic perfectly plastic beams that can withstand normal, shearing, bending

and twisting loadings. For a cylinder element with two nodes, N_1 and N_2, the contact stiffnesses are defined as:

$$\begin{aligned} k_n &= \frac{E_t A}{L} \\ k_t &= \frac{G_t I_t}{L} \\ k_s &= \frac{12 E_b I_b}{L^3} \\ k_b &= \frac{E_b I_b}{L} \end{aligned} \tag{8}$$

where E_t and E_b are the tensile and bending moduli of the material respectively, G_t is the shear modulus associated with the twisting moment and $L = \|N_1 - N_2\|$ is the length of the beam element.

4 GRIDS

A grid can be generated using a series of nodes connected to an arbitrary number of cylinders. The modelling of a grid involves the implementation of the interaction between non-adjacent cylinders (no common nodes). In order to handle cylinder–cylinder interactions, the contact forces between two cylinders C_1 and C_2 are determined. The distance between two cylinders C_1 and C_2 is calculated as the distance between two segments (Fig. 1), bearing in mind that each cylinder is geometrically represented by the Minkowski sum of a sphere and a segment.

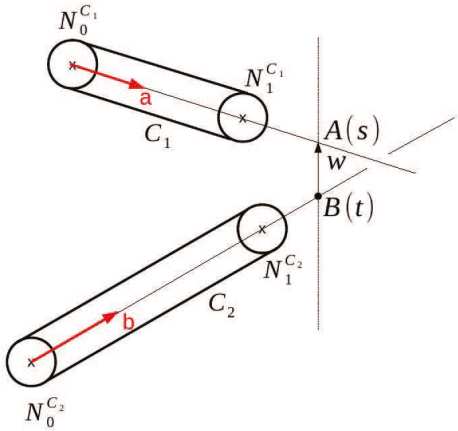

Fig. 1. Distance between two cylinders.

The segments associated to the cylinder C_1 and C_2 are $A = [N_0^{c_1} N_1^{c_1}]$ and $B = [N_0^{c_2} N_1^{c_2}]$ respectively, where $N_j^{c_i}$ correspond to the position of the nodes j of cylinder C_i with

$i \in \{1,2\}$ and $j \in \{1,2\}$. The parametric equations of the segments A and B are:

$$A(s) = N_0^{c_1} + s\,\vec{a} \qquad \forall s \in [0,1] \tag{9}$$

$$B(t) = N_0^{c_2} + t\,\vec{b} \qquad \forall t \in [0,1] \tag{10}$$

with $\vec{a}$ and $\vec{b}$ being the direction vectors of the segments A and B. The vector w between A and B can then be calculated as:

$$w(s,t) = A(s) - B(t) \qquad \forall s,t \in [0,1] \times [0,1] \tag{11}$$

The objective is to find (s_C,t_C) $\in [0,1] \times [0,1]$ such that:

$$\vec{w}_C = w(s_C,t_C) = A(s_C) - B(t_C) = \min_{(s,t)\in[0,1]\times[0,1]} w(s,t) \tag{12}$$

The segment $[A_C B_C]$ is uniquely defined as simultaneously perpendicular to both lines if the segments A and B do not intersect or are not parallel. This implies that the vector $\vec{w}_C = w(s_C,t_C)$ is uniquely perpendicular to the segment vector of the directions of $\vec{a}$ and $\vec{b}$ and the conditions $\vec{a}\cdot\vec{w}_C = 0$ and $\vec{b}\cdot\vec{w}_C = 0$ are satisfied. Hence, the following system of equations can be written:

$$\begin{cases} \vec{w}_C = A(s_C) - B(t_C) \\ \vec{a}\cdot\vec{w}_C = 0 \\ \vec{b}\cdot\vec{w}_C = 0 \end{cases} \tag{13}$$

The solution of Eq. (13) is given by:

$$\begin{cases} s_C = \dfrac{(\vec{a}\cdot\vec{b})(\vec{b}\cdot\vec{w}_0) - \|\vec{b}\|(\vec{a}\cdot\vec{w}_0)}{\|\vec{a}\|\|\vec{b}\| - (\vec{a}\cdot\vec{b})^2} \\ t_C = \dfrac{\|\vec{a}\|(\vec{b}\cdot\vec{w}_0) - (\vec{a}\cdot\vec{b})(\vec{a}\cdot\vec{w}_0)}{\|\vec{a}\|\|\vec{b}\| - (\vec{a}\cdot\vec{b})^2} \end{cases} \tag{14}$$

where $\vec{w}_0 = N_0^{C_1} - N_0^{C_2}$.

For a cylinder–cylinder contact each cylinder is associated to a virtual sphere at the contact point. This approach is similar to the sphere–cylinder contact. The virtual spheres S_{C_1} and S_{C_2} are centred respectively in $A(s_c)$ and $B(t_c)$. Contact laws can then be inherited, and the force and moment linearly distributed on each cylinder node.

5 PFACET ELEMENTS

The grid model described in Section 4 is extended to model arbitrary deformable objects. To achieve this objective a new element is introduced, the so-called PFacet (particle

facet). The PFacet element is geometrically constructed by the Minkowsky sum of a triangular facet and a sphere. It is composed of 3 nodes (spheres) and 3 connections (cylinders). The deformation is defined by the set of positions and orientations of its nodes. The constitutive behaviour of the PFacet element is simulated via an ordinary interaction law acting between the 3 nodes. The mass of the PFacet is equally lumped into the 3 nodes. The introduction of the PFacet element involves the consideration of the following three interactions: sphere–PFacet, cylinder–PFacet and PFacet–PFacet.

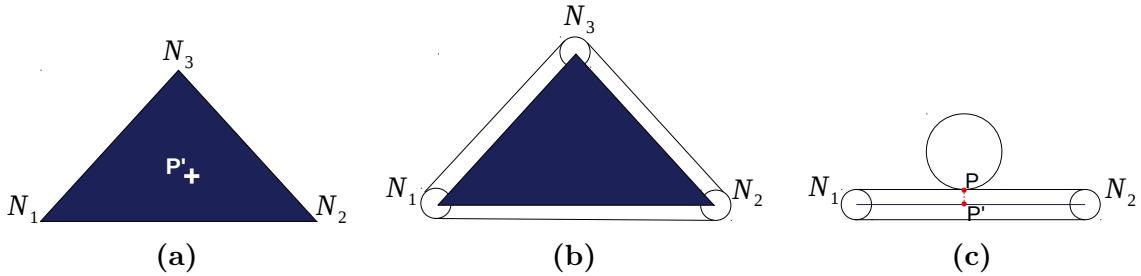

Fig. 2. (a) Triangular skeleton with the nodes, (b) PFacet geometry where the blue zone corresponds to the inside of the PFacet element and (c) P' projection of the contact point P on the plane that contains the PFacet nodes.

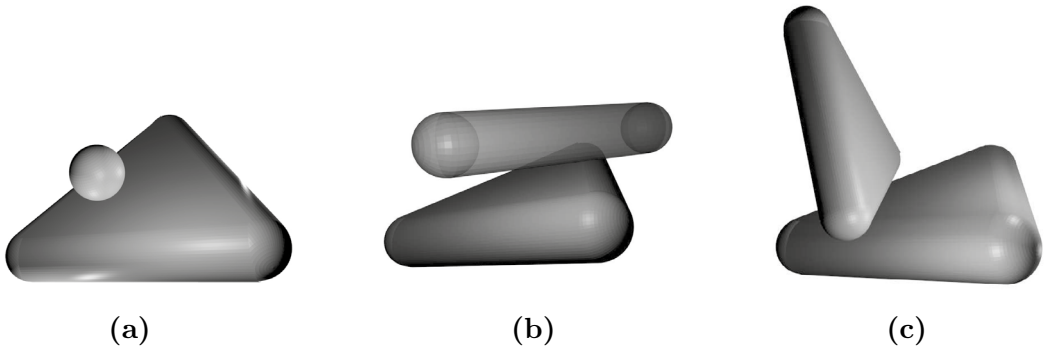

Fig. 3. (a) Sphere–PFacet interaction, (b) Cylinder–PFacet interaction, and (c) PFacet–PFacet interaction.

For a sphere–PFacet interaction (Fig. 3a), the coordinates of the contact point P are characterised by the position of the 3 PFacet nodes. The point P' is the projection of the contact point P (Fig. 2c) on the plane containing the nodes of the PFacet element. The barycentric coordinates (p_1,p_2,p_3) of the point P' (Fig. 2a) are defined as:

$$
\begin{aligned}
p_1 &= \frac{\|\overrightarrow{N_1N_3}\|(\overrightarrow{N_1N_2}\cdot\overrightarrow{N_1P'}) - (\overrightarrow{N_1N_2}\cdot\overrightarrow{N_1N_3})(\overrightarrow{N_1N_3}\cdot\overrightarrow{N_1P'})}{\|\overrightarrow{N_1N_2}\|\|\overrightarrow{N_1N_3}\| - (\overrightarrow{N_1N_2}\cdot\overrightarrow{N_1N_3})(\overrightarrow{N_1N_2}\cdot\overrightarrow{N_1N_3})} \\
p_2 &= \frac{\|\overrightarrow{N_1N_2}\|(\overrightarrow{N_1N_3}\cdot\overrightarrow{N_1P'}) - (\overrightarrow{N_1N_2}\cdot\overrightarrow{N_1N_3})(\overrightarrow{N_1N_2}\cdot\overrightarrow{N_1P'})}{\|\overrightarrow{N_1N_2}\|\|\overrightarrow{N_1N_3}\| - (\overrightarrow{N_1N_2}\cdot\overrightarrow{N_1N_3})(\overrightarrow{N_1N_2}\cdot\overrightarrow{N_1N_3})} \\
p_3 &= 1 - p_1 - p_2
\end{aligned}
\tag{15}
$$

The barycentric coordinates of P' are used to distinguish if the contact is inside the PFacet element (the blue zone in Fig. 2b) or not. If $p_1 \geq 0$ and $p_2 \geq 0$ and $p_3 < 1$, the contact is characterised as inside the PFacet element otherwise a sphere–cylinder interaction is considered. The virtual sphere s'_P is positioned in P'. Both, the virtual sphere and the PFacet element have the same radius. The PFacet element radius is defined as the radius of the PFacet node located at the ends of each cylinder. The virtual sphere's displacement and rotation are linearly interpolated between the 3 nodes of the PFacet N_1, N_2 and N_3.

The translational ($\vec{v}'_P$) and rotational ($\vec{\omega}'_P$) velocities are then calculated from the translational ($\vec{v}_{N_1}$, $\vec{v}_{N_2}$ and $\vec{v}_{N_3}$) and rotational ($\vec{\omega}_{N_1}$, $\vec{\omega}_{N_2}$ and $\vec{\omega}_{N_3}$) velocities of the three nodes:

$$
\begin{aligned}
\vec{v}'_P &= p_1\vec{v}_{N_1} + p_2\vec{v}_{N_2} + p_3\vec{v}_{N_3} \\
\vec{\omega}'_P &= p_1\vec{\omega}_{N_1} + p_2\vec{\omega}_{N_2} + p_3\vec{\omega}_{N_3}
\end{aligned}
\tag{16}
$$

Introducing a virtual sphere s'_P allows the use of the contact model for a classical sphere–sphere interaction. The contact force, $\vec{F}$, is calculated for the virtual sphere and then the force is distributed over the nodes as follows:

$$
\vec{F}_{N_i} = p_i\vec{F} \tag{17}
$$

where $\vec{F}_{N_i}$ is the force applied at the node N_i with $i \in \{1, 2, 3\}$.

A cylinder–PFacet contact (Fig. 3b) is decomposed into a node–PFacet (i.e. sphere–PFacet) contact between the nodes of the cylinder and the PFacet, and a cylinder–cylinder contact between the cylinder and PFacet cylinders.

A PFacet–PFacet interaction (Fig. 3c), is a combination of node–PFacet and cylinder–cylinder interactions. All these types of interactions have been described above.

6 VALIDATION

A tube of length l (Fig. 4a) is subjected to a bending moment. The cylinder is fixed at one end, precisely the nodes initially positioned at $x = 0$ are only fixed along the x-axis. The bending moment M_b is applied at the other end ($x = l$). A distribution of forces $\{f_1 \dots f_{N_l}\}$ such that $\sum_{k=1}^{k=N_l} f_k = 0$ and $\sum_{k=1}^{k=N_l} x_k\, f_k = M_b$ is applied on each nodes which

are initially positioned at $x = l$. The forces f_k are linear in y in the initial configuration. The forces are updated constantly during the deformation to reflect the positions x_k in the deformed state. M_b is increased progressively in order to plot the load–displacement relation. The changes of M_b are sufficiently slow to maintain a quasi-static regime of deformation.

The hollow cylinder is potentially able to buckle in bending. For the boundary conditions presented above, the relevant buckling limit is defined in [10]. It corresponds to an ovalisation of the cross section. The maximum bending moment is calculated as:

$$M_b^{max} = \frac{2\sqrt{2}K_n}{9(1-\nu^2)}d \tag{18}$$

where K_n is the stiffness of the beam in tension, ν is the Poisson's ratio of the wall, and d is the thickness of the wall. This expression is used for comparison in Fig. 4e. In the calculation of M_b^{max}, the values of K_n and ν are obtained from a simulated tension test on the same tube.

When a non-linear displacement is detected in the simulation, the applied moment is kept constant. The buckling is identified when, for a given moment M_b, the deformation of the cylinder increase with time. During the buckling phenomenon, the cylinder enters a dynamic mode of deformation. Finally, the tube reaches an equilibrium via a winding mechanism (Fig. 4d). In the simulation, buckling is reached for a moment value close to the theoretical limit. One can observe that the final state involves self-interaction in the tube (Fig. 4d). It shows that the method developed allows to investigate complex post-buckling behaviours. In addition, the capability of solving problems involving self interacting structures and large deformations is as well demonstrated.

7 EXAMPLE

In the following section a potential application of the developed discrete model is presented. The ability to simulate deformable objects is investigated by simulating a impact of a sphere on a tube. The tube is deformable and composed of 640 PFacet elements with a radius of 2 mm. The tube has a radius of $R = 0.1$ m and a length of 0.8 m. The material parameters used for the tube are: Young's modulus $E_t = 1$ MPa and Poisson's ratio $\nu_t = 0.3$.

The impacting sphere is first modelled by a solid sphere (Fig. 5a) and then by a hollow deformable sphere represented by 128 PFacet elements with a radius of 2 mm (Fig. 5a). The material parameters of the sphere are: Young's modulus $E_s = 100$ MPa and Poisson's ratio $\nu_s = 0.3$. The sphere has a radius $R = 0.1$ m and an impact velocity of $v = 2$ m/s. To focus on the deformation of the impact gravity was not applied during the simulation.

Fig. 5b and Fig. 5c illustrate the final state of the tube after impact of the solid sphere. The tube is deformed and the sphere is stopped with the creation of a crater. The deformation of the tube almost corresponds to its radius. Fig. 6b and Fig. 6c show

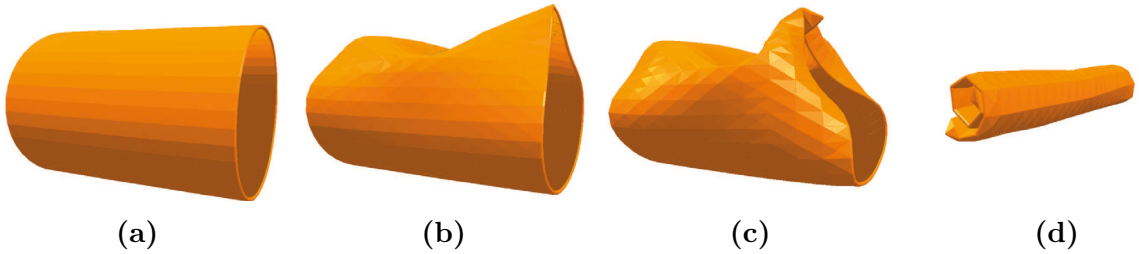

(a) (b) (c) (d)

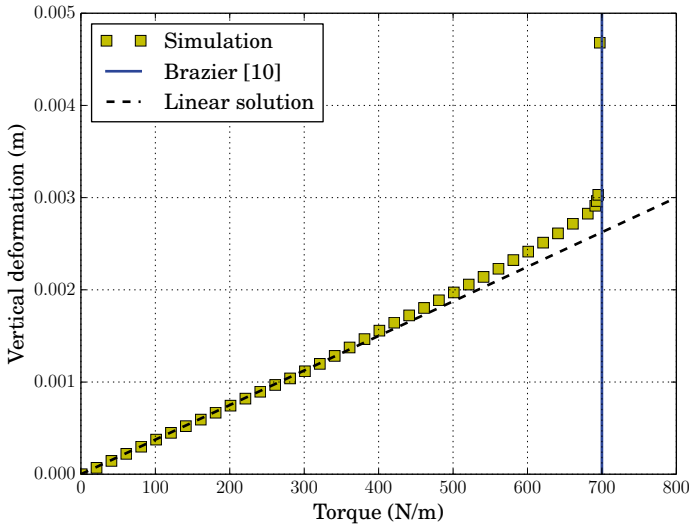

(e)

Fig. 4. Buckling of a tube subjected to an end bending moment: (a)–(d) deformation and (e) comparison with theoretical limit.

the final state of the tube after impact of the deformable sphere. It can be seen that the tube is not as deformed as in the previous case and the impacting sphere deforms itself.

8 CONCLUSIONS

The paper presents a method for the simulation of arbitrary deformable objects. The model is an extension of the flexible cylinder element described in [7]. A new element is introduced into the open-source framework YADE [8]. The so-called PFacet (particle facet) is an element geometrically constructed by the Minkowsky sum of a triangular facet and a sphere. Contact detection is based on the three primitives: sphere, cylinder and facet. It allows the representation of arbitrary deformable structures by using the standard contact models for spheres. The ability of the model to reproduce the behaviour of a structure under bending is validated. A tube subjected to an end bending moment is investigated and an excellent agreement with the theoretical buckling limit is observed.

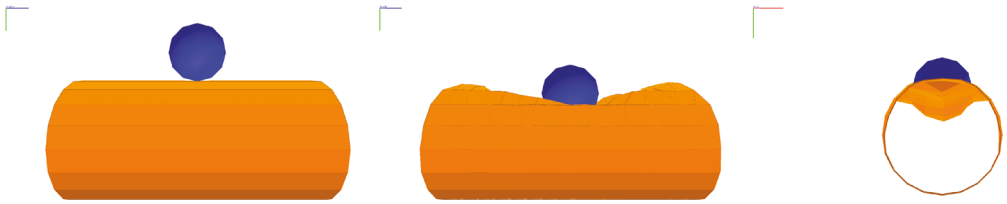

(a) (b) (c)

Fig. 5. Solid sphere impacting on tube: (a) initial state before impact, and (b) front view and (c) side view of final state.

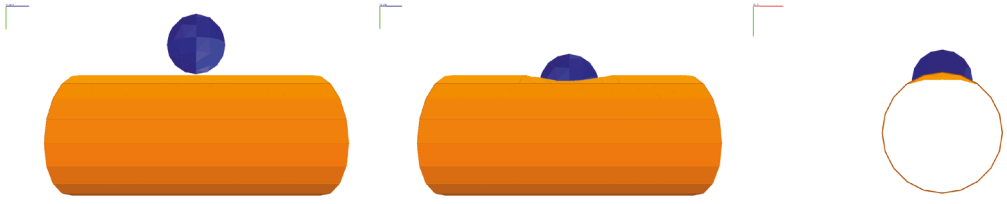

(a) (b) (c)

Fig. 6. Hollow deformable sphere impacting on tube: (a) initial state before impact, (b) front view and (c) side view of final state.

Finally, an example of a sphere (solid and hollow) impacting on a tube is presented. Results show that the model is capable of capturing large deformations and to efficiently simulate complex deformable shapes and soil inclusion problems.

REFERENCES

[1] Radja, A., Dubois, F., (editors). *Discrete-element Modeling of Granular Materials*. ISTE Ltd, London; (2011).

[2] Donzé, F., Richefeu, V., Magnier, S.. Advances in discrete element method applied to soil, rock and concrete mechanics. *Electronic Journal of Geotechnical Engineering* (2009) **8**:1–44.

[3] Galindo-Torres, S., Alonso-Marroquín, F., Wang, Y., Pedroso, D., Muñoz Castaño, J.. Molecular dynamics simulation of complex particles in three dimensions and the study of friction due to nonconvexity. *Physical Review E* (2009) **79**:060301–1–4.

[4] Chareyre, B., Villard, P.. Dynamic spar elements and discrete element methods in two dimensions for the modeling of soil-inclusion problems. *Journal of Engineering Mechanics* (2005) **131**(7):689–698.

[5] Pournin, L., Liebling, T.. A generalization of distinct element method to tridimen-

sional particles with complex shape. In: *Powders and Grains 2005*; vol. 2. (2005), p. 1375–1378.

[6] Alonso-Marroquín, F.. Spheropolygons: A new method to simulate conservative and dissipative interactions between 2D complex-shaped rigid bodies. *Europhysics Letters* (2008) **83**(1):14001–1–14001–6.

[7] Bourrier, F., Kneib, F., Chareyre, B., Fourcaud, T.. Discrete modeling of granular soils reinforcement by plant roots. *Ecological Engineering* (2013) **61**:646–657.

[8] Effeindzourou, A., Chareyre, B., Thoeni, K., Giacomini, A., Kneib, F.. Modelling of deformable structures in the general framework of the discrete element method. *Geotextiles and Geomembranes* (2015) [under review, submitted on 09/12/2014].

[9] Šmilauer, V., Catalano, E., Chareyre, B., Dorofenko, S., Duriez, J., Gladky, A., et al. Yade Reference Documentation. In: Šmilauer, V., (editor). *Yade Documentation*. The Yade Project; 1st ed.; (2010), `http://yade-dem.org/doc/`.

[10] Brazier, L.. On the flexure of thin cylindrical shells and other thin sections. *Proceedings of the Royal Society of London Series A* (1927) **116**(773):104–114.